Research Article

pISSN 2799-8525 · eISSN 2799-8681
J Powder Mater 2026;33(2):130-136

Journal of
Powder Materials

Analysis of Sintering Behavior and Microstructure of Mo-Ta Alloy under Different Sintering Conditions

Byungheon Oh[1], Geon Kim[1], Jio Yoon[1], Dongju Lee[1,2,*]

[1]Department of Urban, Energy, and Environmental Engineering, Chungbuk National University, Chungdae-ro 1, Seowon-Gu, Cheongju, Chungbuk 28644, Republic of Korea
[2]Department of Advanced Materials Engineering, Chungbuk National University, Chungdae-ro 1, Seowon-Gu, Cheongju, Chungbuk 28644, Republic of Korea

Molybdenum-tantalum (Mo-Ta) alloy sputtering targets are widely used in electronic applications owing to their excellent corrosion resistance, high thermal and electrical conductivity, and low electrical impedance. In this study, the sintering behavior and microstructural evolution of Mo-Ta alloys fabricated by spark plasma sintering (SPS) were investigated as a function of sintering temperature in the range of 1650-1800 °C. X-ray diffraction and microstructural analyses indicate that densification and alloying of the mixed Mo and Ta powders occur simultaneously during the SPS process. Increasing the sintering temperatures significantly enhances densification, and the compact sintered at 1750 °C achieves a relative density exceeding 99%, which is essential for high-quality sputtering target applications. The sintered alloys exhibit a clear temperature-dependent grain growth behavior together with a homogeneous microstructure and randomly oriented grains. These results demonstrate that appropriate control of sintering temperature enables the fabrication of dense and microstructurally uniform Mo-Ta alloys, providing valuable guidelines for optimizing sputtering target performance.

Keywords: Molybdenum; Tantalum; Alloy; Spark plasma sintering (SPS)

Received: March 12, 2026
Revised: April 26, 2026
Accepted: April 26, 2026

***Corresponding author:**
Dongju Lee
E-mail: dongjulee@chungbuk.ac.kr

1. Introduction

Molybdenum (Mo) is an outstanding thin-film material for electronic information applications thanks to its high melting point, high electrical conductivity, easy chemical patterning, and good thermal stability [1, 2]. For these reasons, Mo is widely used as a sputtering target material in various electronic components, including thin-film transistor-liquid crystal displays (TFT-LCDs), touch screens, flat-panel displays, electrodes and wiring materials for thin-film solar cells, and barrier layers for semiconductors [3, 4]. However, Mo is susceptible to oxidation at high temperatures. Since thin films are often exposed to temperatures up to approximately 350 °C during device fabrication, oxidation or deterioration of Mo films can significantly degrade the performance of the devices [5, 6]. Therefore, improving the oxidation resistance of Mo while maintaining an adequate wet-etching rate remains an important research challenge [7].

The addition of tantalum (Ta) to Mo enhances its high temperature oxidation resistance, mechanical stability, high thermal conductivity, and low coefficient of thermal expansion [8]. Previous studies have shown that Mo-Ta alloys exhibit higher corrosion resistance than pure Mo [9, 10]. As a result, Mo-Ta alloys are considered promising materials for applications in electronics, nanotechnology, sensors, and gate electrodes for TFT-LCD devices [11].

Mo-based alloy thin films are typically fabricated by magnetron sputtering, which is one of the most widely used physical vapor deposition techniques [12, 13]. In this process, the microstructure of the sputtering target plays a crucial role in determining the quality of the deposited films. Parameters such as target purity, relative density, grain size, and grain orientation must be carefully controlled to achieve the desired film properties [3, 14-16].

Conventional melting and casting methods are commonly

https://doi.org/10.4150/jpm.2026.00080
© 2026 The Korean Powder Metallurgy & Materials Institute

used to produce metal sputtering targets; however, additional thermomechanical processes such as rolling are often required to control the microstructure [17, 18]. Moreover, the melting/casting method is less suitable for refractory metals and alloys with very high melting points, such as Mo, Ta, and their alloys [19, 20]. Powder metallurgy provides an alternative route for producing fine-grained and relatively uniform microstructures, although achieving sufficiently high density remains a challenge.

The spark plasma sintering (SPS) technique enables the production of dense sintered compacts with small grain sizes at relatively low temperatures, and with heating rate exceeding 100 K/min. Furthermore, the pressure applied to loaded powders, and the fast heating and cooling rates, allow the production of targets with a relative density close to the theoretical density [21, 22]. Compared to conventional sintering methods applying external pressure like Hot Pressing (HP) or Hot-Isostatic-Pressing (HIP), densification by SPS is extremely fast. Thus, the sintering temperatures can be lower which limits the grain growth [23-25].

In this study, the sintering behavior of Mo-10 wt.% Ta alloys fabricated by spark plasma sintering (SPS), a rapid densification technique, was investigated at sintering temperatures ranging from 1650 to 1800 °C under a pressure of 50 MPa. The Mo-Ta alloy nanopowder was produced via reduction process of the oxide powders and mixing with pure nanopowders. The Mo-Ta alloy powders were prepared through the reduction of oxide powders followed by mixing with Ta nanopowders. The relative density, grain size, and crystallographic orientation of the sintered compacts were analyzed to clarify the effects of sintering temperature on the densification behavior and microstructural evolution of Mo-10 wt.% Ta alloys produced by powder metallurgy.

2. Experimental

2.1. Materials

MoO_3 powder (purity: 99.9%, particle size: ~200 nm) and Ta nanopowders (purity: 99.99%, particle size: ~100 nm) were purchased from Avention (Siheung, South Korea). Potassium hydroxide (purity: 95%) was obtained from Samchun (Daejeon, South Korea), and potassium ferricyanide (purity: 99.9%) was purchased from Aladdin (Shanghai, China). All chemicals were used as received without further purification.

2.2. Preparation of Mo-Ta alloy nanopowders

MoO_3 and Ta powders were used as starting materials to prepare Mo-Ta alloy powders. The MoO_3 nanopowders were first reduced in a hydrogen atmosphere at 900 °C for 2 h with a heating rate of 10 °C min^{-1} to obtain metallic Mo powders. Subsequently, the reduced Mo powders were mixed with Ta nanopowders at a composition corresponding to Mo-10 wt.% Ta. Then, the powder mixture, together with 6 mm diameter tungsten carbide (WC) balls, was loaded into a polypropylene (PP) bottle and mixed using a horizontal tumbler ball mill at a rotational speed of 180 rpm for 2 h, with a fixed ball-to-powder weight ratio of 7:1.

2.3. Consolidation of the Mo-10 wt.% Ta nanopowders

The Mo-10 wt.% Ta mixed powders (9 g) were loaded into a graphite die with an inner diameter of 15 mm. The die was coated with boron nitride (BN) to suppress reactions with the graphite mold and to facilitate sample removal after sintering. All powder handling procedures were conducted in a glove box (J-924A; JISICO, Seoul, South Korea) to prevent oxidation. Spark plasma sintering (SPS) was performed using an SPS apparatus (JP/SPS-1030; Welltech, Korea). A uniaxial pressure of 50 MPa was applied, and sintering was carried out at temperatures of 1650, 1700, 1750, and 1800 °C for a fixed holding time of 2.5 min under vacuum. The heating rate was maintained at 100 °C/min. After sintering, the compacts were ground and polished using diamond abrasives down to a final particle size of 0.25 μm.

2.4. Characterization

The microstructures and elemental distributions of the Mo-10 wt.% Ta powders and sintered compacts were examined using focused ion beam-scanning electron microscopy (FIB-SEM; Crossbeam 540, Zeiss, Oberkochen, Germany). For further microstructural analysis, the polished samples were chemically etched for 10 s using Murakami's reagent, consisting of potassium hydroxide (10 g), potassium ferricyanide (10 g), and distilled water (100 mL).

Phase identification was conducted by X-ray diffraction (XRD; SmartLab, Rigaku, Tokyo, Japan). Grain sizes were measured by image analysis using ImageJ software (National Institutes of Health, Bethesda, MD, USA), and grain orientation was analyzed by electron backscatter diffraction (EBSD) equipped in an ultra-high-resolution field-emission scanning electron microscope (UHR FE-SEM; SU8230, Hitachi, Tokyo, Japan). The relative densities of the sintered compacts were determined using the Archimedes method, based on a theoretical density of 10.633 g/cm^3.

3. Results and Discussion

Fig. 1 presents the microstructures and phase characteristics of both the starting powders and the mixed powders used for the preparation of the Mo-10 wt.% Ta alloy. Fig. 1(a) shows the SEM image of the hydrogen-reduced Mo powders. The reduced Mo particles exhibit an irregular morphology with angular and faceted features, forming loosely agglomerated clusters. The particle surfaces appear relatively rough, and a broad particle size distribution is observed, corresponding to agglomerated Mo powder clusters. Fig. 1(b) presents the SEM image of the Ta powders. In contrast to the reduced Mo powders, the Ta particles display a predominantly spherical morphology with relatively smooth surfaces. The particle size of the raw powders was determined from SEM images using ImageJ software. The average particle sizes were 349.39 ± 147.72 nm for Mo powder and 105.14 ± 78.89 nm for Ta powders. Fig. 1(c) shows the SEM image and corresponding energy-dispersive X-ray spectroscopy (EDS) elemental mapping of the mixed Mo-10 wt.% Ta powders after low-energy ball milling. The mixed powders exhibit a composite morphology in which irregular Mo particles and spherical Ta particles are homogeneously distributed. The EDS analysis confirms the presence of Mo and Ta elements, and their compositions are consistent with the nominal Mo-10 wt.% Ta mixing ratio, indicating effective mixing without noticeable elemental segregation. Fig. 1(d) presents the X-ray diffraction (XRD) patterns of the reduced Mo powders, Ta powders, and the mixed Mo-10 wt.% Ta powders. The diffraction peaks correspond to the body-centered cubic (BCC) phases of Mo and Ta. The characteristic reflections observed at 2θ = 40.3°, 58.5°, 73.6°, and 87.5° can be indexed to the (110), (200), (211), and (220) planes of the BCC Mo-Ta structure, respectively. No secondary phases or oxide-related peaks are detected, confirming the phase purity of the starting powders and the successful preparation of the Mo-10 wt.% Ta mixed powders.

Fig. 2 shows the surface microstructures and corresponding elemental distributions of the Mo-10 wt.% Ta sintered compacts consolidated at different sintering temperatures for a

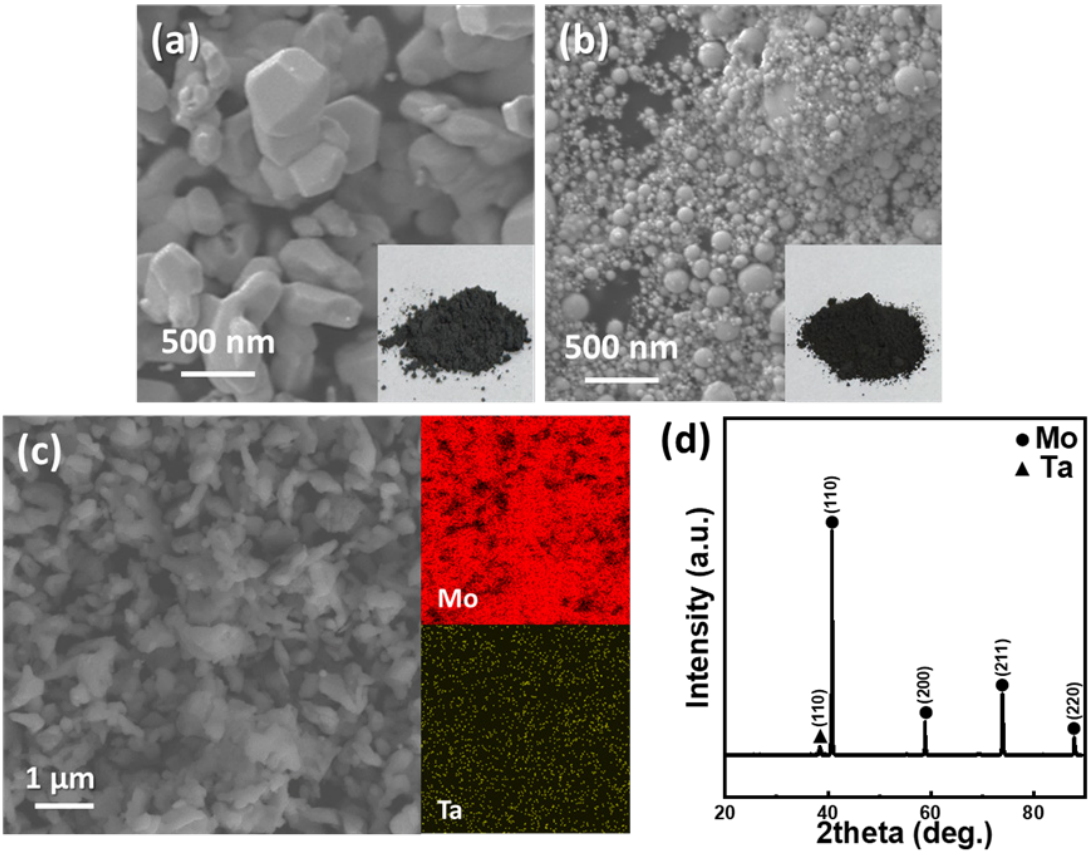


Fig. 1. SEM images of the starting powders and mixed Mo-Ta powder: (a) hydrogen-reduced Mo nanopowders, (b) Ta nanopowders, and (c) SEM image and corresponding EDS elemental mapping of the mixed Mo-10 wt.% Ta nanopowders after ball milling. The elemental maps confirm the homogeneous distribution of Mo and Ta in the mixed powder. (d) XRD pattern of the mixed Mo-10 wt.% Ta nanopowders.

holding time of 2.5 min. At lower sintering temperatures of 1650 and 1700 °C, surface pores are observed and the elemental distributions of Mo and Ta exhibit local inhomogeneity, indicating limited densification and alloying (Fig. 2a-d). At sintering temperatures of 1750 °C and above, no visible pores are observed, and the elemental distributions of Mo and Ta are relatively uniform (Fig. 2e-h). These results suggest that increasing the sintering temperature promotes densification and enhances alloying between Mo and Ta.

Fig. 3a shows the XRD patterns of the Mo-10 wt.% Ta compacts sintered by SPS at different temperatures. The diffraction patterns of all sintered samples exhibit characteristic peaks at 2θ = 40.3, 58.4, 73.4, and 87.3°, which can be indexed to the (110), (200), (211), and (220) planes of the body-centered cubic (BCC) Mo-Ta alloy, respectively [26-28]. No additional diffraction peaks corresponding to the individual Mo or Ta phases, or to secondary phases such as molybdenum carbide or tantalum carbide, are detected. These results clearly indicate that the initially mixed Mo and Ta powders are effectively alloyed during the SPS sintering process, forming a single-phase Mo-Ta solid solution. Fig. 3b presents the relative densities of the Mo-10 wt.% Ta compacts as a function of sintering temperature. The relative density increases with increasing sintering temperature, and the compacts sintered at temperatures of 1750 °C and above exhibit relative densities exceeding 99%, indicating near-full densification. In contrast, samples sintered at lower temperatures show insufficient densification. The simultaneous achievement of high relative density and single-phase alloy formation demonstrates that SPS effectively promotes both densification and alloying of the mixed Mo-Ta powders at elevated sintering temperatures [29]. Fig. 3c-g show the grain size distributions for samples sintered at different temperatures, clearly indicating an increase in grain size with increasing sintering temperatures.

Fig. 4 presents the etched microstructures of the Mo-10 wt.% Ta sintered compacts consolidated at different sintering temperatures A clear increase in grain size is observed with increasing sintering temperatures, indicating enhanced grain growth at higher temperatures. The compacts sintered at 1650 and 1700 °C (Fig. 4a and 4b, respectively) exhibit relatively fine grains with limited grain growth, suggesting restricted grain boundary mobility at these temperatures. The average grain sizes at 1650 °C and 1700 °C are approximately 6.25 and 9.00 μm, respectively. The grain morphology remains comparatively uniform, and grain coarsening is not pronounced. At a sintering temperature of 1700 °C (Fig. 4b), a noticeable increase in grain size is observed, with the average grain size increasing from 6.25 to 9.00 μm. Further grain coarsening occurs at 1750 °C (Fig. 4c) and 1800 °C (Fig. 4d), with average grain sizes of approximately 10.67 and 11.07 μm, respectively, although the growth rate becomes more gradual [21]. Compared with conventional sintering methods such as hot pressing (HP) and hot isostatic pressing

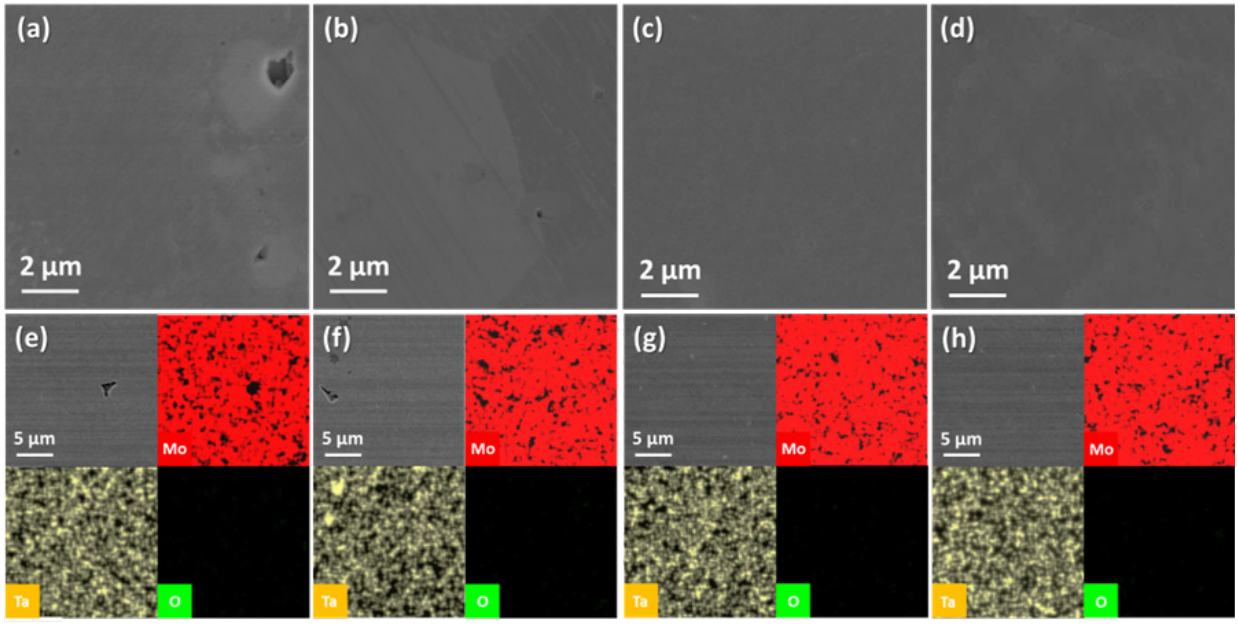


Fig. 2. (a-d) SEM images and (e-h) corresponding EDS elemental maps of Mo-10 wt.% Ta compacts sintered at 1650, 1700, 1750, and 1800 °C, respectively.

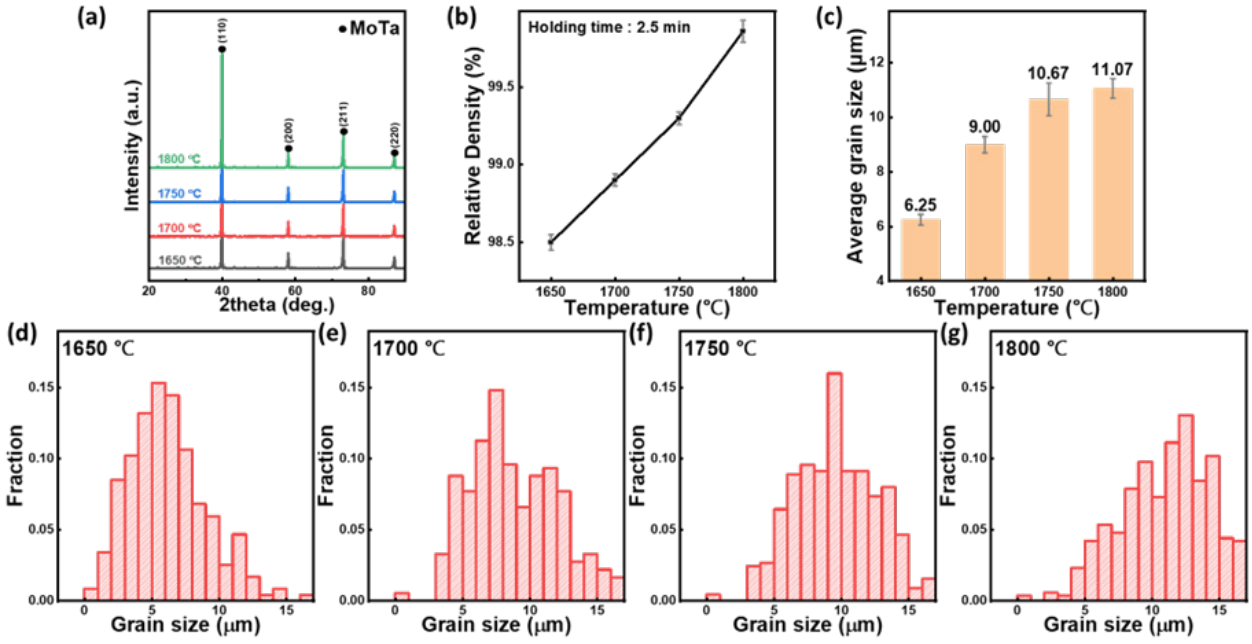


Fig. 3. (a) XRD patterns, (b) relative densities, and (c) average grain size of Mo-10 wt.% Ta compacts sintered according to the sintering temperatures. (d-g) Grain size distributions of the compacts sintered at 1650, 1700, 1750, and 1800 °C, respectively.

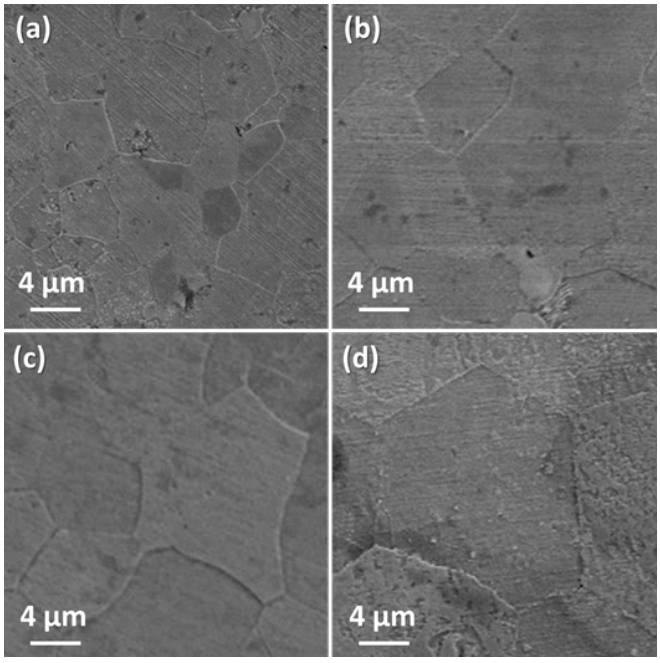


Fig. 4. Etched SEM microstructures of Mo-10 wt.% Ta compacts sintered by SPS at (a) 1650 °C, (b) 1700 °C, (c) 1750 °C, and (d) 1800 °C.

(HIP), SPS employs rapid internal Joule heating, enabling much faster densification within a few minutes. This suppresses excessive and abnormal grain growth, resulting in a finer, more uniform, and randomly oriented microstructure, whereas HP and HIP often lead to grain coarsening and possible texture development due to prolonged thermal exposure associated with longer sintering times [30]. The evolution of grain size with sintering temperature is primarily attributed to enhanced atomic diffusion and increased grain boundary mobility at elevated temperatures. Unlike high-energy ball milling processes such as mechanical alloying, which can induce severe plastic deformation and irregular particle morphologies due to intensive crushing and friction, the low-energy milling route employed in this study preserves a relatively uniform powder morphology. This facilitates controlled grain growth and uniform microstructure development during sintering [31, 32].

Fig. 5 presents the EBSD analysis results of the Mo-10 wt.% Ta sintered compacts. With increasing sintering temperatures, the average grain size progressively increased to 6.25, 9.00, 10.67, and 11.07 μm, respectively, exhibiting a trend consistent with the grain growth induced by elevated sintering temperatures, as discussed previously. This trend is consistent with the grain size evolution observed from the etched surface analysis, demonstrating good agreement between the two characterization methods. Fig. 5(a) shows the EBSD image quality (IQ) map of the sample sintered at 1750 °C, revealing an equiaxed grain structure with well-defined grain boundaries. The corresponding inverse pole figure (IPF) maps along the X, Y, and Z

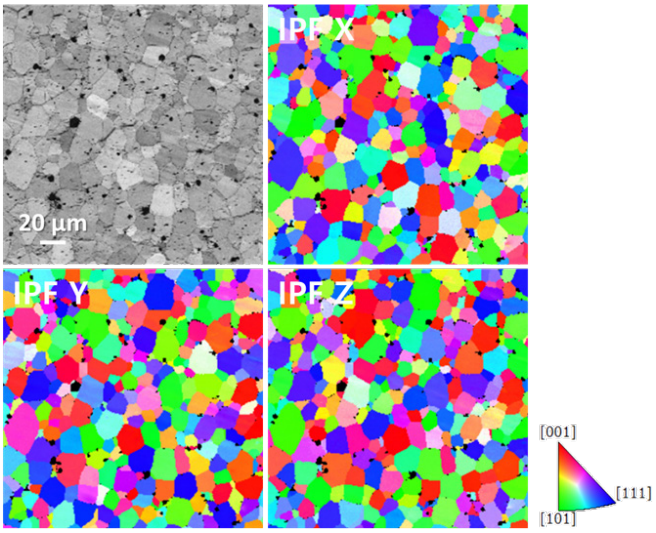


Fig. 5. EBSD results of the Mo-10 wt.% Ta compact sintered at 1750 °C: (a) EBSD image quality (IQ) map and (b-d) inverse pole figure (IPF) maps along the X, Y, and Z directions, respectively.

directions show no preferred crystallographic orientation, indicating a randomly oriented grain structure. This confirms that no strong texture is introduced during the SPS process, even at elevated sintering temperatures. The combination of homogeneous grain growth with increasing sintering temperatures and random crystallographic orientation suggests that the microstructure of the Mo-10 wt.% Ta alloy is well controlled. For sputtering target applications, a dense microstructure is beneficial for stable plasma discharge, uniform sputtering erosion, and suppress arc formation and particle ejection during sputtering, enabling more stable processing. Such a microstructure is advantageous for sputtering target applications, as it is expected to enable more uniform sputtering behavior. In particular, the absence of strong texture and the presence of uniformly distributed grains are considered promising for achieving improved sputtering rates and sputtering efficiency, as well as for realizing high-quality thin films with fewer defects. Furthermore, the dense and uniform microstructure is expected to enhance corrosion resistance by minimizing porosity and reducing pathways for environmental attack.

4. Conclusion

The sintering behavior and microstructural evolution of Mo-Ta alloys fabricated by spark plasma sintering were investigated as a function of sintering temperature. The initially mixed Mo and Ta powders were effectively alloyed during the SPS process, forming a single-phase body-centered cubic (BCC) Mo-Ta solid solution. Compacts sintered at temperatures of 1750 °C and above achieved relative densities exceeding 99%, whereas those sintered at lower temperatures showed insufficient densification. Grain size increased with increasing sintering temperatures, and EBSD analysis confirmed a randomly oriented grain structure consistent with etched surface observations. Considering the balance between densification and grain growth, 1750 °C for 2.5 min was identified as the optimal sintering condition. These results demonstrate that appropriate control of sintering parameters enables the fabrication of dense and microstructurally uniform Mo-Ta alloys with strong potential for sputtering target applications.

Funding

This work was supported by the Korea Institute of Energy Technology Evaluation and Planning (KETEP) grant funded by the Korea government (MOTIE, 20217510100020, Development of platform process using common core and materialization technology for rare metal recovery from industrial low-grade waste liquid).

Conflict of Interest

The authors have no conflicts of interest to declare.

Data Availability Statement

Data will be made available on request.

Author Information and Contribution

Byungheon Oh: M.S. candidate; Investigation, Data curation, Formal analysis, Visualization, Writing - original draft.

Geon Kim: Integrated M.S.-Ph.D candidate; Investigation, Formal analysis.

Jio Yoon: M.S. candidate; Investigation, Formal analysis.

Dongju Lee: Associate Professor; Project administration, Conceptualization, Supervision, Writing - review & editing, Funding acquisition.

Acknowledgments

None.

References

[1] P. Chelvanathan, S. Shahahmadi, F. Arith, K. Sobayel, M. Aktharuzzaman, K. Sopian, F. Alharbi, N. Tabet and N. Amin: Thin solid films, **638** (2017) 213.

[2] H. Zhao, J. Xie, A. Mao, A. Wang, Y. Chen, T. Liang and D. Ma: Materials, **11** (2018) 1634.

[3] B.-J. Lee, K.-B. Lee, M.-H. Cheon, D.-W. Seo and J.-W. Choi: Coatings, **13** (2023) 1070.

[4] H. Li, G. Q. Yang, X. Y. Hu, Y. H. Hu, R. B. Zeng, J. R. Cai, L. Q. Yao, L. M. Lin, L. P. Cai and G. Chen: Adv. Sci., **10** (2023) 2303414.

[5] A. List, C. Mitterer, G. Mori, J. Winkler, N. Reinfried and W. Knabl, In: In Proc. 17th International Plansee Seminar; (2009) p. 1.

[6] N. Birks, G. H. Meier and F. S. Pettit, Introduction to the high temperature oxidation of metals, Cambridge University Press, (2006) 1.

[7] J. Li, Z. Fu, L. Wei, G. Zhang, S. Wei, L. Xu, K. Pan, J. Shen and J. Yang: Int. J. Refract. Met. Hard Mater., **103** (2022) 105770.

[8] A. M. Hofer, G. Mori, A. Fian, J. Winkler and C. Mitterer: Thin Solid Films, **599** (2016) 1.

[9] B. Chen, N. Biswas and V. Misra: J. Electrochem. Soc., **153** (2006) G417.

[10] J. Zhou, F. Chen, C. Zhang, C. Su, H. Zhang and S. Guo: Surf. Coat. Technol., **489** (2024) 131108.

[11] S.-H. Lee, B. O. Kim and J. H. Seo: J. Nanosci. Nanotechnol., **15** (2015) 7770.

[12] B.-H. Seo, H. Kim, H. Choe, J.-H. Jeon, J. Winkler, Y. Lee, S.-H. Kim and J. H. Seo: Sci. Adv. Mater., **8** (2016) 854.

[13] C. V. Ramana, V. V. Atuchin, V. Kesler, V. Kochubey, L. Pokrovsky, V. Shutthanandan, U. Becker and R. C. Ewing: Appl. Surf. Sci., **253** (2007) 5368.

[14] N. Dhar, P. Chelvanathan, M. Zaman, K. Sopian and N. Amin: Energy Procedia, **33** (2013) 186.

[15] H.-S. Huang, H.-C. Tung, C.-H. Chiu and I.-T. Hong: China Steel Tech. Rep., **26** (2013) 59.

[16] K. Yu, X. Xue, L. Xu, G. Li, X. Zhang and Y. Wang: Int. J. Refract. Met. Hard Mater., **126** (2025) 106948.

[17] S. Raggl, J. Postler, J. Winkler, G. Strauss, C. Feist, A. Plankensteiner, M. Eidenberger-Schober and P. Scheier: J. Vac. Sci. Technol. A, **35** (2017) 061308.

[18] J.-K. Chen, B.-H. Tsai and H.-S. Huang: Mater. Trans., **56** (2015) 665.

[19] R.-X. Song, D. Wang, Y. Yang, J. He, S. Li, H.-L. Yan and L. Zuo: Materials, **18** (2025) 3235.

[20] H. Zhang, Y. Zhao, S. Huang, S. Zhu, F. Wang and D. Li: Materials, **12** (2019) 720.

[21] Y. Le Godec and S. Le Floch: Materials, **16** (2023) 997.

[22] P. Cavaliere, B. Sadeghi and A. Shabani, Spark plasma sintering: process fundamentals. In Spark plasma sintering of materials: advances in processing and applications, Springer, (2019) 3.

[23] M. Omori: Mater. Sci. Eng. A, **287** (2000) 183.

[24] W. Chen, U. Anselmi-Tamburini, J. Garay, J. Groza and Z. Munir: Mater. Sci. Eng. A, **394** (2005) 132.

[25] U. Anselmi-Tamburini, S. Gennari, J. Garay and Z. Munir: Mater. Sci. Eng. A, **394** (2005) 139.

[26] B. Xiao, Y. Lysogorskiy, A. Savan, H. Bögershausen, J. Pfetzing-Micklich, D. Raabe, R. Drautz and A. Ludwig: High Entropy Alloys Mater., **1** (2023) 110.

[27] D. Liu, X. Yang, L. Huang, Y. Pan and J. Zhang: Journal of Wuhan University of Technology-Mater. Sci. Ed., **38** (2023) 1248.

[28] D. Liu, J. Zhang, L. Huang, S. Li, B. Nong, Y. Jin and Y. Pan: Philos. Mag. Lett., **102** (2022) 359.

[29] G. Cao, C. Estournes, J. Garay and R. Orru, Spark plasma sintering: current status, new developments and challenges, Elsevier, (2019).

[30] B. Zhang, M. Wei, Y. Huang and J. Wang: J. Alloys Compd., (2025) 184787.

[31] W. Hu, Z. Dong, L. Yu, Z. Ma and Y. Liu: J. Mater. Sci. Technol., **36** (2020) 84.

[32] P. Li, C. Chen, C. Zhang, N. Xiao, H. Zhang, Y. Li and Z. Guo: High Temp. Mater. Processes, **40** (2021) 361.